Site-Specific Characterization of the N-Linked Glycans of Murine Prion Protein by High-Performance Liquid Chromatography/Electrospray Mass Spectrometry and Exoglycosidase Digestions†

Elaine Stimson,‡,§ James Hope,§ Angela Chong,§ and Alma L. Burlingame*,‡,||

Ludwig Institute for Cancer Research, 91 Riding House Street, London, U.K., BBSRC Institute for Animal Health, Compton, Berkshire RG20 7NN, U.K., Department of Pharmaceutical Chemistry, University of California at San Francisco, San Francisco, California 94143, and Department of Biochemistry and Molecular Biology, University College London, London, U.K.

Received September 29, 1998; Revised Manuscript Received January 20, 1999

ABSTRACT: The murine prion protein PrP gene encodes a protein of 254 amino acids with two consensus sites for Asn-linked glycosylation at codons 180 and 196. A partial site-specific study of the N-linked glycans from hamster PrP has previously been carried out by mass spectrometry [Stahl, N., Baldwin, M. A., Teplow, D. B., Hood, L., Gibson, B. W., Burlingame, A. L., and Prusiner, S. B. (1993) *Biochemistry 32*, 1991−2002] and revealed that the glycosylation at Asn-181 (equivalent to mouse 180) is heterogeneous, comprising over 30 glycoforms. The identification of the glycosylated peptide spanning Asn-197 was not reported. Recent technical advances in electrospray mass spectrometry now provide the sensitivity to detect low femtomole quantities of glycopeptides with >5000 mass resolution and 30 ppm mass measurement [Medzihradszky, K. F., Besman, M. J., and Burlingame, A. L. (1998) *Rapid Commun. Mass Spectrom. 12*, 472−478]. This performance coupled with stepwise exoglycosidase digestion has been employed to establish the differential nature of the structural complexity (glycoforms) of the glycans at Asn-180 and Asn-196 from a single strain infected with the ME7 strain. Some sixty structures have been found characterized by neutral and sialylated bi-, tri-, and tetraantennary complex-type bearing outer-arm α(1−3)-fucosylation (the Lewis^x and sialyl-Lewis^x epitopes), core α(1,6) fucosylation, and the presence of terminal HexNAc residues. The Lewis^x trisaccharide is the major nonreducing structure at Asn-180, and significant amounts of both Lewis^x and sialyl Lewis^x epitopes are observed at Asn-196. The abundance of the Lewis^x and sialyl Lewis^x epitopes on murine PrP^{Sc} may indicate a role for these structures in the normal function of PrP^C or the pathophysiology of PrP^{Sc}.

Transmissible spongioform encephalopathies are progressive neurodegenerative diseases of humans and animals, which can be transmitted via contaminated food or by inoculation. Survival time, clinical signs, and brain pathology depend primarily on the genetics of the host and the strain of the infecting agent (or prion). Many different strains of agent from natural cases of ovine (scrapie) or bovine spongioform encephalopathy have been characterized by their phenotypes in a panel of inbred mice (*1*). In all cases, conversion of a normal isoform of the plasma membrane protein, PrP,[1] to an aggregated insoluble, proteolytically resistant form (designated PrP^{Sc}) is a key feature of molecular pathogenesis of these diseases (*2*).

The mouse PrP gene encodes a protein of 254 amino acids with two consensus sites for Asn-linked glycosylation at codons 180 and 196. Previous characterization of the glycans of hamster PrP by anion-exchange chromatography, exoglycosidase digestion, and methylation analysis revealed heterogeneous, complex-type oligosaccharides, some of which possessed terminal sialic acids and fucosylated antennae (*3*). This study proposed that such a diversity of oligosaccharide structures would permit the occurrence of over 400 different forms of the scrapie prion protein. Earlier studies of the N-linked glycans from hamster PrP have previously been carried out by mass spectrometry (*4*) and revealed that the glycosylation at Asn-181 (equivalent to mouse 180) is heterogeneous, comprising over 30 glycoforms. In addition, analysis by capillary electrophoresis showed that a high proportion of these oligosaccharides are neutral. However, the identification of the glycosylated peptide spanning Asn-197 was not accomplished using the mass spectrometers available at that time. Recent technical advances in electrospray mass spectrometry now provide the sensitivity required

† This work was supported by the Ludwig Institute for Cancer Research, London Branch, and by the NIH National Center for Research Resources, Grant RR 01614 (to A.L.B.).

* Address correspondence to this author at the Department of Pharmaceutical Chemistry, University of California, 513 Parnassus Ave., San Francisco, CA 94143-0446. Tel (415) 476-5641; Fax (415) 476-0688; Email alb@itsa.ucsf.edu.

‡ Ludwig Institute for Cancer Research.

§ BBSRC Institute for Animal Health.

|| UCSF and University College London.

[1] Abbreviations: PrP, prion protein; PrP^{Sc}, scrapie isoform of the prion protein; HPLC, high-performance liquid chromatography; ESI-MS, electrospray ionization mass spectrometry; ESI-oaTOF-MS, electrospray ionization orthogonal acceleration time-of-flight mass spectrometry; Hex, hexose; Fuc, fucose; HexNAc, *N*-acetylhexosamine; NeuAc, *N*-acetylneuraminic acid; TIC, total ion current.

10.1021/bi982330q CCC: $18.00
Published on Web 03/23/1999

to detect low femtomole quantities of glycopeptides with >5000 mass resolution and 30 ppm mass measurement (*5*). We have employed this new generation of electrospray mass spectrometric instrumentation as well as exoglycosidase digestion to determine the first site-specific characterization of the microheterogeneity of both N-linked glycan sites of murine PrP^{Sc}.We report a comprehensive structural analysis of all the complex carbohydrate structures attached to both Asn-180 and Asn-196 on murine PrP^{Sc} from a single mouse strain infected with the ME7 strain of scrapie.

MATERIALS AND METHODS

Purification of PrP^{Sc}. PrP^{Sc} was purified from mouse brains by detergent lysis, differential centrifugation and size-exclusion chromatography according to the procedure described by Hope et al. (*6*).

Alkylation and Tryptic Digestion. Purified PrP^{Sc} was reduced in dithiothreitol (Pierce) and alkylated with 4-vinyl pyridine (Sigma) in the presence of 6 M guanidine hydrochloride, pH 8.5 (*7*). The alkylated protein was precipitated with methanol, redissolved in 4 M urea and 200 mM ammonium bicarbonate, pH 8.5, and digested with trypsin (Promega) (5% trypsin by weight overnight at 37 °C).

Sequential Exoglycosidase Digestions. Digestions were carried out on purified glycopeptides: Neuraminidase (from *Vibrio cholerae*, EC 3.2.1.18, Boehringer Mannheim), broad specificity 50 milliunits in 100 μL of 50 mM ammonium acetate buffer, pH 5.5, for 48 h, with a fresh aliquot added after 24 h; α-fucosidase (from *Xanthomonas manihotis*, New England Biolabs), specificity for α(1,3/4)-fucose 0.2 unit in 100 μL of provided incubation buffer for 24 h; β-galactosidase (from *Diplococcus pneumonaie*, Boehringer Mannheim), specificity for β(1,4)Gal 10 milliunits in 100 μL of provided incubation buffer for 24 h with a fresh aliquot of enzyme added after 12 h. All enzyme digestions were carried out at 37 °C and terminated by centrifugal evaporation. An appropriate aliquot was taken after each digestion and analyzed by capillary LC-ESMS using the Mariner oaTOF mass spectrometer described below.

Liquid Chromatography Electrospray Mass Spectrometry. Microbore and capillary HPLC/ESI-MS experiments were performed with both electrospray triple quadrupole (PE Sciex 300) and an electrospray orthogonal acceleration time-of-flight (ESI-oaTOF) (Mariner, PE Biosystems) mass spectrometers, respectively. Glycopeptides were detected selectively by microbore LC-ESMS equipped with selected ion monitoring for sugar oxonium ions (*8, 9*). This was performed with an ABI 140B dual syringe pump system set to deliver mobile phase at 40 μL/min. The tryptic digest mixture in urea was injected (Rheodyne model 8125) onto a Vydac microbore column (C18, 1 mm × 150 mm, 5 μ) and separation was achieved by use of an alcohol-based mobile phase (*10*) where solvent A was 0.1% formic acid in H_2O and solvent B was ethanol−*n*-propanol in 0.05% formic acid (5:2 v/v). The column was equilibrated in solvent A containing 5% solvent B, and the gradient was initiated 10 min after injection and then increased linearly to 60% B over 60 min. The column effluent was monitored at 214 nm by a UV detector (ABI 785A) equipped with a high-sensitivity U−Z flow cell (LC Packings, San Francisco), after which it was split so that approximately 5 μL/min was directed into the Sciex mass spectrometer and 35 μL/min was collected manually and saved for further characterization. The mass spectrometer was scanned in both the conventional and SIM mode. For the latter experiment the carbohydrate oxonium ions at *m*/*z* 204 ($HexNAc^+$), *m*/*z* 292 ($NeuAc^+$) and *m*/*z* 366 ($HexHexNAc^+$) (dwell time, 200 ms each) were monitored at a high orifice potential of 200 V. Full scans at *m*/*z* 383−2500 (0.125 AMU steps, scan time 5 s) were then acquired at a lower orifice potential of 75 V.

The collected HPLC fractions containing glycopeptides were pooled, dried down, resuspended in 0.1% formic acid in H_2O, and reanalyzed by capillary HPLC coupled to a Mariner electrospray-orthogonal acceleration TOF mass spectrometer (PE Biosystems, Framingham, MA). Capillary HPLC was achieved by use of a 140C dual syringe pump flowing at 10−12 μL/min that was stream-split so that 1−2 μL/min flowed onto the column (180 μm × 50 mm, LC Packings). After sample injection, the column was eluted with a linear gradient of 0.5%/min of the alcohol-based mobile phase described above, and the HPLC eluent was monitored at 210 nm by a UV detector (ABI 785A) that was fitted with a capillary U−Z flow cell (LC-Packings). The HPLC was interfaced to the electrospray source of the Mariner by a length of fused silica capillary tubing. A scan was acquired every 3 s as the result of 24 000 pulses, over a mass range of *m*/*z* 360−2000. Singly and doubly protonated ions of gramicidin S were used for a two-point external calibration.

RESULTS

Glycopeptides containing glycosylation sites at Asn-180 and Asn-196 were isolated from tryptic digests of PrP^{Sc} by microbore HPLC/ESIMS using a Sciex 300 triple quadrupole mass spectrometer that was scanned in both the conventional and selected ion monitoring (SIM) mode. For the SIM experiment, the orifice voltage was adjusted to 200 V (from 75 V) and the mass spectrometer was set to monitor the mass values representing specific carbohydrate fragment ions characteristic of the presence of generic glycopeptides (*8, 9, 11*). These SIM data (not shown) revealed the elution profiles of two different glycopeptide-containing fractions at approximately 37 and 47 min.

The earlier-eluting glycopeptide profile was significantly broader than the later peak, and analysis of its mass profile revealed peptide heterogeneity due to two different factors—incomplete proteolysis and in vitro modification of an N-terminal glutamine. Bulky carbohydrate chains at Asn-196 apparently prevent attack by trypsin at Lys-193, because only limited cleavage at this site was observed, confined to protein bearing either no N-linked glycosylation or only the small glycan structures (partial mouse protein sequence ^{163}RPVDQYSNQNNFVHDCV^{180}NITI^{184}KQHTVTT-TT^{193}KGE^{196}NFTETDV^{203}K). The major tryptic site found accessible in this region occurred at Lys-184, liberating a tryptic peptide Gln_{185}−Lys_{203} bearing an N-terminal glutamine residue. This Gln-185 residue was observed to be partially converted to pyroGlu during mass spectral analysis, thus accounting for the observation of an unusually broad chromatographic profile due to the presence of three glycopeptides containing Asn-180—pyroGln_{185}−Lys_{203}, Gln_{185}−Lys_{203}, and Gly_{194}−Lys_{203}—that were chromatographically

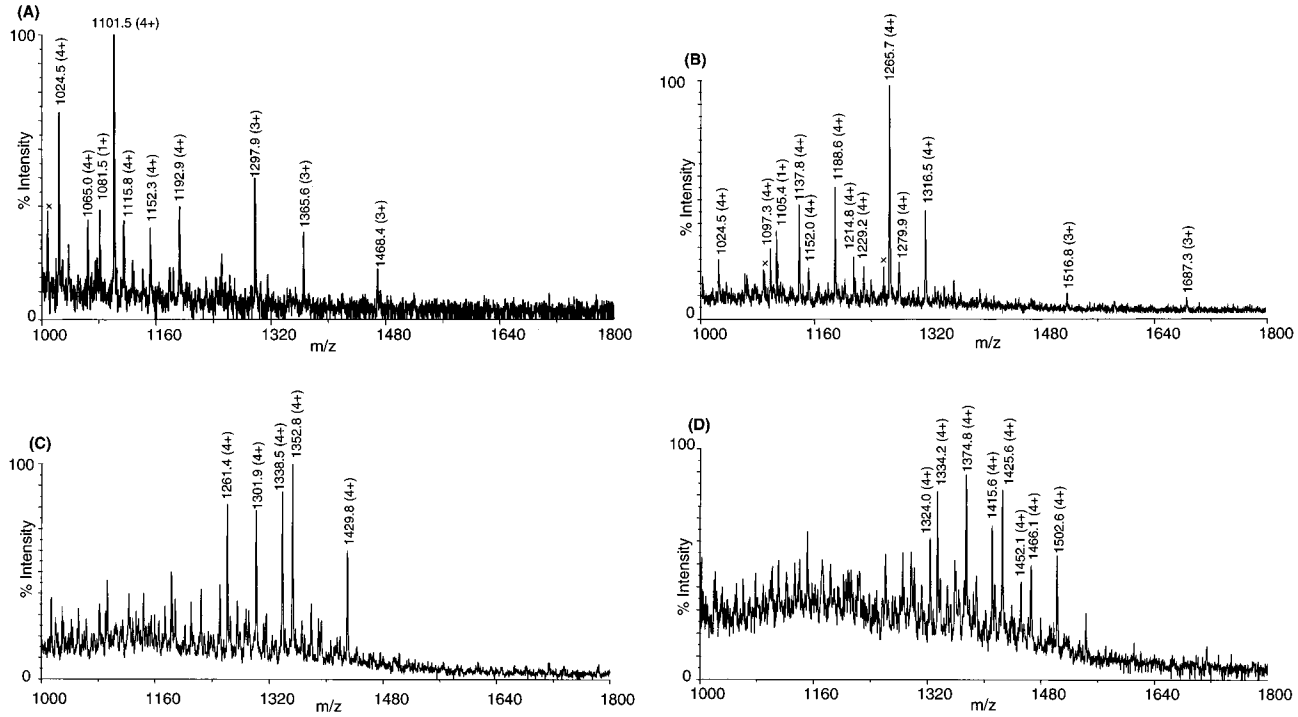

FIGURE 1: ESI-oaTOF mass spectra of the tryptic glycopeptides containing PrP residues $Q_{185}-K_{203}$ (MW_{avg} = 2137.3 Da), which contain a consensus sequence for N-linked glycosylation at Asn-196. Electrospray mass spectrum of the (A) asialyl, (B) monosialyl, (C) disialyl, and (D) trisialyl glycopeptides.

unresolved. Of these three, the predominant glycopeptide species contained the amino acid sequence $Gln_{185}-Lys_{203}$. Therefore, for the sake of simplicity, this Asn-180 glycopeptide was chosen for mass spectral interpretation and discussion (see below).

The narrow profile of the later eluting fraction was due to charge heterogeneity from differential sialylation (*10*). In these experiments large signals were detected for both unglycosylated peptides and this provided unambiguous evidence for partial occupancy of both glycosylation sites as previously suggested (*6*, *12*). However, the unglycosylated partial tryptic peptide ($Gln_{185}-Lys_{203}$) was not detected, indicating that Lys-193 is completely digested when Asn-196 is not glycosylated.

To ensure detection of all glycoforms attached to each N-linked site, the two sets of pooled HPLC fractions containing putative Asn-196 and Asn-180 glycopeptides were analyzed separately by capillary HPLC/ESI-oaTOF-MS.

Asparagine 196 Site. The ESI-oaTOF spectra for the Asn-196 glycopeptides are shown in Figure 1. The separation of differentially sialylated species is clearly evident in the alcohol-based solvent system employed as resported earlier (*10*), with the least sialylated glycoform eluting first [i.e., the peaks at *m*/*z* 1192.9 in Figure 1A and *m*/*z* 1265.7 in Figure 1B differ by 72.8, the *m*/*z* of the 4+ charge state of a NeuAc residue, indicating that the former glycopeptide (*m*/*z* 1192.9) has one less sialic acid than the latter glycopeptide (*m*/*z* 1265.7)]. The average mass values (*13*) were determined for molecular ions for all Asn-196 glycopeptides because low ion statistics gave unresolved isotope peaks. Therefore, subtraction of the calculated average mass of the peptide $Gln_{185}-Lys_{203}$ (MW = 2137.3) from the average molecular masses of the glycopeptides observed provided the oligosaccharide residue compositions and stoichiometry summarized in Table 1. The structural class of each oligosaccharide was tentatively assigned by comparison of the oligosaccharide compositions with the carbohydrate structures reported previously for hamster PrP^{Sc} (*3*) and those known to occur in mammalian glycoproteins. These compositions suggest that complex-type oligosaccharides that bear up to three sialic acid residues occur at the N-linked consensus site at Asn-196. The asialo glycopeptides elute first (Figure 1A), followed sequentially by the mono- (Figure 1B), di- (Figure 1C), and trisialylated (Figure 1D) components. However, not all structural isomers are neutral, mono-, di-, and trisialylated; e.g., some structures are neutral or can be capped with only one or two sialic acid residues ($Hex_6HexNAc_6Fuc_3$, $Hex_6HexNAc_6Fuc_3NeuAc$, and $Hex_6HexNAc_6Fuc_3NeuAc_2$, respectively). The relative abundance of the molecular ion signals suggest that the major components at this site are monosialylated. Earlier glycopeptide studies have indicated that when glycopeptides with the same peptide sequence and different oligosaccharide components are compared, the relative intensities in the ESI-MS data correlate closely with the relative quantities of each glycoform (*14*). The oligosaccharide compositions also suggest that bisecting GlcNAc is likely to be present; e.g., $Hex_7HexNAc_7Fuc_3NeuAc_2$ corresponds to a tetraantennary structure with bisecting GlcNAc, although a pentaantennary oligosaccharide with a nonreducing terminal GlcNAc residue cannot be completely ruled out.

Asparagine 180 Site. Analysis of three sets of mass spectral data (summarized in Table 2) obtained by capillary HPLC/ESI-oaTOF-MS of the pooled HPLC fractions of glycopeptides occurring at the Asn-180 site corresponded to the separated, differentially sialylated glycoforms present. Thus, subtraction of the mass of the tryptic peptide spanning residues 156−184 (average mass 3638.1) from the measured mass of each putative glycopeptide yielded the tentative glycan compositions presented in Table 2. The carbohydrate composition for the most abundant signal in the asialo mass

Table 1: HPLC/Electrospray Mass Spectrometry Data Obtained from Sequential Exoglycosidase Digestion of the Sialylated Glycopeptides (Q/pyroE_{185}−K_{203}) Spanning Asn-196

intact glycopeptides (Gln-185)				after α-sialidase (*V. cholerae*) digestion (Gln-185)			after α-fucosidase and β-galactosidase digestion (pyroGlu-185)	
m/*z*	glycopeptide MW_{avg}	carbohydrate MW_{avg}	proposed glycan composition	*m*/*z*	glycopeptide MW_{avg}	carbohydrate MW_{avg}	*m*/*z*	glycopeptide MW_{avg}
1297.9 [3+]	3890.7	1771.6	$Hex_4HexNAc_4Fuc_2$	1297.9 [3+]	3890.6	1771.6	1189.5 [3+]	3565.4
1024.5 [4+]	4093.8	1974.8	$Hex_4HexNAc_5Fuc_2$	1024.5 [4+]	4093.8	1974.8	1257.2 [3+]	3768.6
1365.6 [3+]				1365.6 [3+]				
1065.0 [4+]	4256.0	2137.0	$Hex_5HexNAc_5Fuc_2$	1065.0 [4+]	4256.0	2137.0	1257.2 [3+]	3768.6
1101.5 [4+]	4402.1	2283.1	$Hex_5HexNAc_5Fuc_3$	1101.5 [4+]	4402.1	2283.1	1257.2 [3+]	3768.6
1468.4 [3+]				1468.4 [3+]				
1115.8 [4+]	4459.2	2340.2	$Hex_5HexNAc_6Fuc_2$	1115.8 [4+]	4459.2	2340.2	1324.9 [3+]	3971.7
				1487.4 [3+]				
1152.3 [4+]	4605.3	2486.3	$Hex_5HexNAc_6Fuc_3$	1152.3 [4+]	4605.2	2486.3	1324.9 [3+]	3971.7
1192.9 [4+]	4767.6	2648.5	$Hex_6HexNAc_6Fuc_3$	1192.9 [4+]	4767.6	2648.5	1324.9 [3+]	3971.7
1097.3 [4+]	4385.0	2266.0	$Hex_4HexNAc_5Fuc_2NeuAc$	1024.5 [4+]	4093.8	2137.0	1257.2 [3+]	3768.6
				1365.6 [3+]				
1137.8 [4+]	4547.2	2428.2	$Hex_5HexNAc_5Fuc_2NeuAc$	1065.0 [4+]	4256.0	2137.0	1257.2 [3+]	3768.6
1516.8 [3+]				1419.7 [3+]				
1152.0 [4+]	4604.3	2485.3	$Hex_5HexNAc_6FucNeuAc$	1079.3 [4+]	4313.0	2194.0	1324.9 [3+]	3971.7
				1438.7 [3+]				
1224.9 [4+]	4895.5	2776.5	$Hex_5HexNAc_6FucNeuAc_2$	1079.3 [4+]	4313.0	2194.0	1324.9 [3+]	3971.7
				1438.7 [3+]				
1251.2 [4+]	5000.6	2881.6	$Hex_6HexNAc_5Fuc_2NeuAc_2$	1105.5 [4+]	4418.1	2299.1	1257.2 [3+]	3768.6
				1473.7 [3+]				
1324.0 [4+]	5291.9	3172.9	$Hex_6HexNAc_5Fuc_2NeuAc_3$	1105.5 [4+]	4418.1	2299.1	1257.2 [3+]	3768.6
				1473.7 [3+]				
1188.6 [4+]	4750.5	2631.5	$Hex_5HexNAc_6Fuc_2NeuAc$	1115.8 [4+]	4459.2	2340.2	1324.9 [3+]	3971.7
1261.4 [4+]	5041.6	2922.6	$Hex_5HexNAc_6Fuc_2NeuAc_2$	1115.8 [4+]	4459.2	2340.2	1324.9 [3+]	3971.7
1334.2 [4+]	5332.9	3213.9	$Hex_5HexNAc_6Fuc_2NeuAc_3$	1115.8 [4+]	4459.2	2340.2	1324.9 [3+]	3971.7
1214.8 [4+]	4855.2	2736.2	$Hex_6HexNAc_5Fuc_3NeuAc$	1142.0 [4+]	4564.2	2445.2	1257.2 [3+]	3768.6
1229.2 [4+]	4912.6	2793.6	$Hex_6HexNAc_6Fuc_2NeuAc$	1156.3 [4+]	4621.3	2502.3	1324.9 [3+]	3971.7
1301.9 [4+]	5203.8	3084.8	$Hex_6HexNAc_6Fuc_2NeuAc_2$	1156.3 [4+]	4621.3	2502.3	1324.9 [3+]	3971.7
1374.8 [4+]	5495.1	3376.1	$Hex_6HexNAc_6Fuc_2NeuAc_3$	1156.3 [4+]	4621.3	2502.3	1324.9 [3+]	3971.7
1265.7 [4+]	5058.8	2939.8	$Hex_6HexNAc_6Fuc_3NeuAc$	1192.9 [4+]	4767.5	2648.5	1324.9 [3+]	3971.7
1338.5 [4+]	5350.0	3231.0	$Hex_6HexNAc_6Fuc_3NeuAc_2$	1192.9 [4+]	4767.5	2648.5	1324.9 [3+]	3971.7
1279.9 [4+]	5115.8	2996.8	$Hex_6HexNAc_7Fuc_2NeuAc$	1207.1 [4+]	4824.5	2705.5	1392.6 [3+]	4174.9
1415.6 [4+]	5658.3	3539.3	$Hex_7HexNAc_6Fuc_2NeuAc_3$	1197.1 [4+]	4748.5	2629.5	1324.9 [3+]	3971.7
1352.8 [4+]	5407.0	3288.0	$Hex_6HexNAc_7Fuc_2NeuAc_2$	1207.1 [4+]	4824.5	2705.5	1392.6 [3+]	4174.9
1425.6 [4+]	5698.3	3579.3	$Hex_6HexNAc_7Fuc_2NeuAc_3$	1207.1 [4+]	4824.5	2705.5	1392.6 [3+]	4174.9
1452.1 [4+]	5804.4	3685.4	$Hex_7HexNAc_6Fuc_3NeuAc_3$	1233.7 [4+]	4930.6	2811.6	1324.9 [3+]	3971.7
1316.5 [4+]	5262.0	3143.0	$Hex_6HexNAc_7Fuc_3NeuAc$	1243.7 [4+]	4970.7	2851.7	1392.6 [3+]	4174.9
1357.0 [4+]	5424.1	3305.1	$Hex_7HexNAc_7Fuc_3NeuAc$	1284.2 [4+]	5132.8	3013.8	1392.6 [3+]	4174.9
1429.8 [4+]	5715.3	3596.3	$Hex_7HexNAc_7Fuc_3NeuAc_2$	1284.2 [4+]	5132.8	3013.8	1392.6 [3+]	4174.9
1466.1 [4+]	5860.5	3741.5	$Hex_7HexNAc_7Fuc_2NeuAc_3$	1247.7 [4+]	4986.7	2867.7	1392.6 [3+]	4174.9
1502.6 [4+]	6006.6	3887.6	$Hex_7HexNAc_7Fuc_3NeuAc_3$	1284.2 [4+]	5132.8	3013.8	1392.6 [3+]	4174.9

spectrum suggests the presence of a biantennary structure bearing bisecting GlcNAc ($Hex_4HexNAc_5Fuc_2$), which has previously been observed as a major component on hamster PrP27−30 (*3*). The observed electrospray mass values also indicate the presence of many other minor asialo di- and triantennary complex structures, possibly occurring both with and without bisecting GlcNAc; e.g., $Hex_6HexNAc_6Fuc_3$ and $Hex_6HexNAc_5Fuc_3$ are likely to be triantennary structures with and without a bisecting GlcNAc residue, respectively. However, for the former oligosaccharide, the presence of a tetraantennary structure with one agalactosyl antenna cannot be disregarded. The sialylated species are likely to include bi-, tri-, and tetraantennary structures with up to two sialic acid residues. Smaller signals were observed for these sialylated structures, implying that they are less abundant than the asialo components.

Exoglycosidase Digestions. To establish that these putative structures are correct for the tentative compositions assigned thus far, the remainder of the purified glycopeptide-containing fractions were incubated sequentially with specific exoglycosidases and analyzed by HPLC/ESI-oaTOF-MS after each step. The mass differences observed after each single exoglycosidase digestion and the monosaccharide substrate specificity of each exoglycosidase were used to establish the sequence of the nonreducing termini. The glycopeptide mixtures were first digested with the nonspecific sialidase from *V. cholerae*. The resulting ESI-oaTOF mass spectra showed the anticipated absence of signals for the sialylated structures concomitant with both the appearance or increase in abundance of their nonsialylated counterparts (summarized in Tables 1 and 2) that now coelute with the neutral constituents observed earlier as noted above. Comparison of the relative abundance of the molecular ions for the neutral and sialidase-treated glycopeptides spanning Asn-196 (lower and upper overlay spectra of Figure 2A, respectively) reveal that the major components at this site contain terminal sialic acid. For example, a significant increase in molecular ion abundance was observed for the asialo structures at *m*/*z* 1065.0 ($Hex_5HexNAc_5Fuc_2$), *m*/*z* 1115.8 ($Hex_5HexNAc_6Fuc_2$), and *m*/*z* 1192.9 ($Hex_6HexNAc_6$-

Table 2: HPLC/Electrospray Mass Spectrometry Data Obtained from Sequential Exoglycosidase Digestion of N-Linked Glycopeptides (Y_{156}−K_{184}) Containing Asn-180[a]

intact glycopeptide					α-fucosidase digestion		β-galactosidase digestion	
m/z								
monoisotopic	average	MW (Da)	carbohydrate $mass_{avg}$ (Da)	carbohydrate assignment	*m/z*	MW_{avg} (Da)	*m/z*	MW_{avg} (Da)
	1017.7 [5+]	5083.5_{avg}	1463.4_{avg}	$Hex_3HexNAc_4Fuc$	1017.7 [5+]	5083.5	1017.7 [5+]	5083.5
	1271.9 [4+]				1271.9 [4+]		1271.9 [4+]	
1057.610 [5+]	1058.3 [5+]	5283.150_{mi}	1665.324_{mi}	**$Hex_3HexNAc_5Fuc$**	1058.3 [5+]	5286.7	1058.3 [5+]	5286.7
1321.803 [4+]	1322.7 [4+]	5286.7_{avg}	1666.6_{avg}		1322.7 [4+]		1322.7 [4+]	
	1079.3 [5+]	5391.7_{avg}	1771.6_{avg}	$Hex_4HexNAc_4Fuc_2$	1050.1 [5+]	5245.6	1017.7 [5+]	5083.5
	1348.9 [4+]				1312.4 [4+]		1271.9 [4+]	
	1352.9 [4+]	5407.7_{avg}	1787.7_{avg}	$Hex_5HexNAc_4Fuc$	1082.5 [5+]	5407.7	1017.7 [5+]	5083.5
					1352.9 [4+]		1271.9 [4+]	
	1090.8 [5+]	5448.4_{avg}	1828.4_{avg}	$Hex_4HexNAc_5Fuc$	1090.8 [5+]	5448.4	1058.3 [5+]	5286.7
					1363.1 [4+]		1322.7 [4+]	
	1111.8 [5+]	5553.8_{avg}	1933.8_{avg}	$Hex_5HexNAc_4Fuc_2$	1082.5 [5+]	5407.7	1017.7 [5+]	5083.5
	1389.5 [4+]				1352.9 [4+]		1271.9 [4+]	
1119.268 [5+]	1120.0 [5+]	5591.340_{mi}	1973.614_{mi}	**$Hex_4HexNAc_5Fuc_2$**	1090.8 [5+]	5448.4	1058.3 [5+]	5286.7
1398.840 [4+]	1399.7 [4+]	5594.9_{avg}	1974.8_{avg}		1363.1 [4+]		1322.7 [4+]	
	1131.4 [5+]	5652.0_{avg}	2032.0_{avg}	$Hex_4HexNAc_6Fuc$	1131.4 [5+]	5652.0	1099.0 [5+]	5489.8
	1414.0 [4+]				1414.0 [4+]		1373.5 [4+]	
	1426.0 [4+]	5700.7_{avg}	2080.7_{avg}	$Hex_5HexNAc_4Fuc_3$	1082.5 [5+]	5407.7	1017.7 [5+]	5083.5
	1141.0 [5+]				1352.9 [4+]		1271.9 [4+]	
	1152.4 [5+]	5757.0_{avg}	2137.0_{avg}	$Hex_5HexNAc_5Fuc_2$	1123.2 [5+]	5610.9	1058.3 [5+]	5286.7
					1403.7 [4+]		1322.7 [4+]	
	1160.6 [5+]	5798.1_{avg}	2178.1_{avg}	$Hex_4HexNAc_6Fuc_2$	1131.4 [5+]	5652.0	1099.0 [5+]	5489.8
	1450.5 [4+]				1414.0 [4+]		1373.5 [4+]	
1180.908 [5+]	1181.6 [5+]	5899.540_{mi}	2281.814_{mi}	**$Hex_5HexNAc_5Fuc_3$**	1123.2 [5+]	5610.9	1058.3 [5+]	5286.7
	1476.8 [4+]	5903.2_{avg}	2283.1_{avg}		1403.7 [4+]		1322.7 [4+]	
	1193.0 [5+]	5960.3_{avg}	2340.2_{avg}	$Hex_5HexNAc_6Fuc_2$	1163.8 [5+]	5814.1	1099.0 [5+]	5489.8
	1491.0 [4+]				1454.5 [4+]		1373.5 [4+]	
	1214.1 [5+]	6065.4_{avg}	2445.3_{avg}	$Hex_6HexNAc_5Fuc_3$	1156.6 [5+]	5778.1	1058.3 [5+]	5286.7
							1322.7 [4+]	
	1222.3 [5+]	6106.4_{avg}	2486.3_{avg}	$Hex_5HexNAc_6Fuc_3$	1163.8 [5+]	5814.1	1099.0 [5+]	5489.8
	1527.6 [4+]				1454.5 [4+]		1373.5 [4+]	
	1243.3 [5+]	6211.5_{avg}	2591.4_{avg}	$Hex_6HexNAc_5Fuc_4$	1156.6 [5+]	5778.1	1058.3 [5+]	5286.7
							1322.7 [4+]	
	1254.7 [5+]	6268.6_{avg}	2648.5_{avg}	$Hex_6HexNAc_6Fuc_3$	1196.3 [5+]	5976.3	1099.0 [5+]	5489.8
					1495.1 [4+]		1373.5 [4+]	

intact glycopeptide				α-sialidase digestion			α-fucosidase and β-galactosidase digestion	
m/z	MW_{avg} (Da)	carbohydrate mass (Da)	carbohydrate assignment	*m/z*	MW_{avg} (Da)	carbohydrate mass (Da)	*m/z*	MW_{avg} (Da)
1149.0 [5+]	5740.1	2120.0	$Hex_4HexNAc_5FucNeuAc$	1090.8 [5+]	5448.4	1828.4	1058.3 [5+]	5286.7
1436.0 [4+]				1363.1 [4+]			1322.7 [4+]	
1189.6 [5+]	5943.2	2323.2	$Hex_4HexNAc_6FucNeuAc$	1131.4 [5+]	5652.0	2032.0	1099.0 [5+]	5489.8
1486.8 [4+]				1414.0 [4+]			1373.5 [4+]	
1210.7 [5+]	6048.3	2428.2	$Hex_5HexNAc_5Fuc_2NeuAc$	1152.4 [5+]	5757.0	2137.0	1058.3 [5+]	5286.7
1513.1 [4+]				1440.3 [4+]			1322.7 [4+]	
1251.3 [5+]	6251.5	2631.5	$Hex_5HexNAc_6Fuc_2NeuAc$	1193.0 [5+]	5960.3	2340.2	1099.0 [5+]	5489.8
1563.9 [4+]				1491.0 [4+]			1373.5 [4+]	
1272.3 [5+]	6356.5	2736.2	$Hex_6HexNAc_5Fuc_3NeuAc$	1214.1 [5+]	6065.4	2445.2	1058.3 [5+]	5286.7
							1322.7 [4+]	
1313.0 [5+]	6559.8	2939.8	$Hex_6HexNAc_6Fuc_3NeuAc$	1254.7 [5+]	6268.6	2648.5	1099.0 [5+]	5489.8
							1373.5 [4+]	
1228.3 [5+]	6136.4	2516.4	$Hex_5HexNAc_4Fuc_2NeuAc_2$	1111.8 [5+]	5553.8	1933.8	1017.7 [5+]	5083.5
				1389.5 [4+]			1271.9 [4+]	
1239.7 [5+]	6193.5	2573.5	$Hex_5HexNAc_5FucNeuAc_2$	1123.2 [5+]	5610.9	1990.9	1058.3 [5+]	5286.7
				1403.7 [4+]			1322.7 [4+]	
1268.9 [5+]	6339.6	2719.6	$Hex_5HexNAc_5Fuc_2NeuAc_2$	1152.4 [5+]	5757.0	2137.0	1058.3 [5+]	5286.7
				1440.3 [4+]			1322.7 [4+]	
1280.3 [5+]	6396.6	2776.5	$Hex_5HexNAc_6FucNeuAc_2$	1163.8 [5+]	5814.1	2194.0	1099.0 [5+]	5489.8
				1454.5 [4+]			1373.5 [4+]	
1301.3 [5+]	6501.6	2881.6	$Hex_6HexNAc_5Fuc_2NeuAc_2$	1184.8 [5+]	5919.1	2299.1	1058.3 [5+]	5286.7
							1322.7 [4+]	
1309.6 [5+]	6542.8	2922.6	$Hex_5HexNAc_6Fuc_2NeuAc_2$	1193.0 [5+]	5960.3	2340.2	1099.0 [5+]	5489.8
				1491.0 [4+]			1373.5 [4+]	
1321.0 [5+]	6599.8	2979.8	$Hex_5HexNAc_7FucNeuAc_2$	1204.5 [5+]	6017.3	2397.3	1139.6 [5+]	5693.0
1342.0 [5+]	6704.9	3084.8	$Hex_6HexNAc_6Fuc_2NeuAc_2$	1225.5 [5+]	6122.4	2502.4	1099.0 [5+]	5489.8
							1373.5 [4+]	
1350.2 [5+]	6746.0	3126.0	$Hex_5HexNAc_7Fuc_2NeuAc_2$	1233.7 [5+]	6163.5	2543.5	1139.6 [5+]	5693.0
				1541.9 [4+]				
1371.2 [5+]	6851.1	3231.0	$Hex_6HexNAc_6Fuc_3NeuAc_2$	1254.7 [5+]	6268.6	2648.5	1099.0 [5+]	5489.8
							1373.5 [4+]	
1382.6 [5+]	6908.2	3288.0	$Hex_6HexNAc_7Fuc_2NeuAc_2$	1266.1 [5+]	6325.7	2705.5	1139.6 [5+]	5693.0
				1582.4 [4+]				

[a] Boldface type indicates the major species identified on the basis of the relative abundance of the molecular ions in the mass spectra. Monoisotopic masses were determined for the major glycoforms; however, average masses were calculated for minor glycopeptides with unresolved molecular ion signals.

Table 3: Y Series Fragment Ions Observed in the CID Spectrum of the N-Linked Glycopeptide ($Y_{156}-K_{184}-Hex_4HexNAc_5Fuc_2$) at *m/z* 1120.0 $[M + 5H]^{5+}$

fragment ion composition (Y series)	*m/z*	observed MW_{mi} (Da)	calculated MW_{mi} (Da)
$Y_{156}-K_{184}-HexNAc$	1280.64 $[M + 3H]^{3+}$ 1920.46 $[M + 2H]^{2+}$	3838.92	3838.81
$Y_{156}-K_{184}-HexNAcFuc$	1329.31$[M + 3H]^{3+}$ 1993.47 $[M + 2H]^{2+}$	3984.93	3984.86
$Y_{156}-K_{184}-HexNAc_2$	1348.34 $[M + 3H]^{3+}$ 2022.01 $[M + 2H]^{2+}$	4042.02	4041.88
$Y_{156}-K_{184}-HexNAc_2Fuc$	1396.99 $[M + 3H]^{3+}$	4187.97	4187.94
$Y_{156}-K_{184}-HexNAc_2Hex$	1402.34 $[M + 3H]^{3+}$	4204.02	4203.94
$Y_{156}-K_{184}-HexNAc_2HexFuc$	1451.00 $[M + 3H]^{3+}$	4350.00	4349.99
$Y_{156}-K_{184}-HexNAc_2Hex_2$	1456.31 $[M + 3H]^{3+}$	4365.93	4365.99
$Y_{156}-K_{184}-HexNAc_3Hex$	1470.03 $[M + 3H]^{3+}$	4407.09	4407.02
$Y_{156}-K_{184}-HexNAc_2Hex_2Fuc$	1505.04 $[M + 3H]^{3+}$	4512.12	4512.05
$Y_{156}-K_{184}-HexNAc_3HexFuc$	1518.66 $[M + 3H]^{3+}$	4552.98	4553.08
$Y_{156}-K_{184}-HexNAc_3Hex_2$	1524.02 $[M + 3H]^{3+}$	4569.06	4569.07
$Y_{156}-K_{184}-HexNAc_2Hex_3Fuc$	1559.38 $[M + 3H]^{3+}$	4675.14	7674.10
$Y_{156}-K_{184}-HexNAc_3Hex_2Fuc$	1572.74 $[M + 3H]^{3+}$	4715.22	4715.13
$Y_{156}-K_{184}-HexNAc_3Hex_3$	1578.13 $[M + 3H]^{3+}$	4731.39	4731.12
$Y_{156}-K_{184}-HexNAc_3Hex_3Fuc$	1626.74 $[M + 3H]^{3+}$	4877.22	4877.18
$Y_{156}-K_{184}-HexNAc_3Hex_3Fuc_2$	1675.45 $[M + 3H]^{3+}$	5023.35	5023.24

Fuc_3) after sialidase digestion, establishing that a large proportion of the natural glycan structures or glycoforms are capped with sialic acid. Furthermore, many sialylated structures do not exist as asialo counterparts, because many new signals appear after neuraminidase digestion [e.g., *m/z* 1105.5 ($Hex_6HexNAc_5Fuc_2$), *m/z* 1156.3 ($Hex_6HexNAc_6Fuc_2$), *m/z* 1207.1 ($Hex_6HexNAc_7Fuc_2$), and *m/z* 1284.2 ($Hex_7HexNAc_7Fuc_3$)]. In contrast, comparison of the relative abundance of the molecular ions for the asialo glycopeptides spanning Asn-180 with their sialidase-digested counterparts (lower and upper overlay spectra of Figure 2B, respectively) indicates that neutral glycoforms are the major natural components at this site. However, a significant difference in signal intensity occurs at *m/z* 1090.8 (5+) ($Hex_4HexNAc_5Fuc$) and *m/z* 1193.0 (5+) ($Hex_5HexNAc_6Fuc_2$), which indicates that these structures are the major sialylated substituents at Asn-180.

Further characterization of the sialidase treated glycopeptides was achieved by exhaustive digestion with α(1−3,4) fucosidase (*X. manihotis*) followed by β-galactosidase (*D. pneumonaie*), with analysis by HPLC/ESI-oaTOF-MS after each step (summarized in Tables 1 and 2). After complete digestion with both enzymes the saccharide moieties were truncated to the following core structures: $Hex_3HexNAc_4Fuc$, $Hex_3HexNAc_5Fuc$, $Hex_3HexNAc_6Fuc$, and $Hex_3HexNAc_7Fuc$, which conform to bi-, tri-, and tetraantennary glycans. All Asn-196 and Asn-180 glycopeptides bear one fucose residue that is resistant to α(1−3,4)-fucosidase digestion. This finding is consistent with α(1,6)-fucose remaining on the chitobiose core. Also, the complete removal of terminal galactose by β-galactosidase (β1,4-specific) indicates the presence of type 2 antennae (*15*) and thus, the sialyl Lewis^x and Lewis^x structural epitopes (*16*).

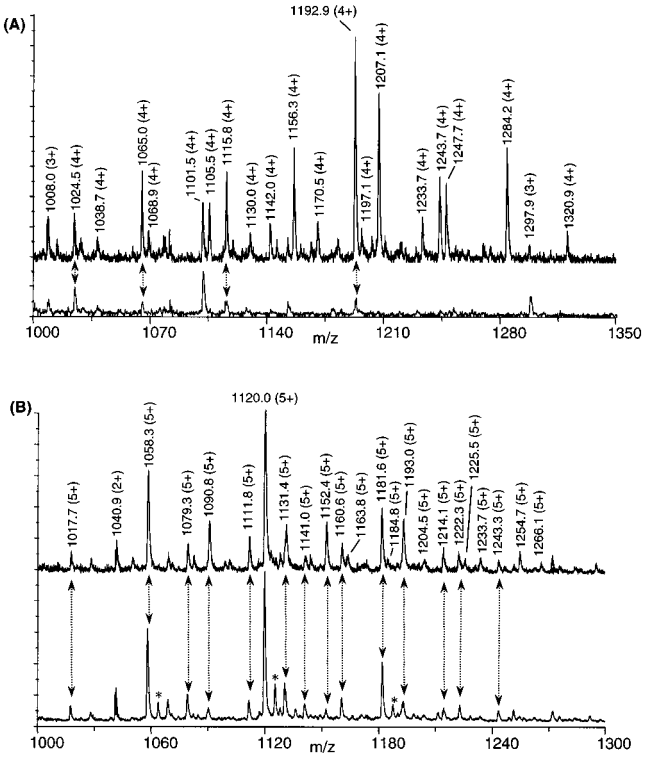

FIGURE 2: Mass spectral comparisons of the asialo and α-sialidase-treated glycopeptides at (A) Asn-196 and (B) Asn-180. The asialo and α-sialidase mass spectra were normalized by using the intensities of the assigned neutral glycopeptides in each spectrum as guides; i.e., no sialylated counterparts for $Hex_5HexNAc_5Fuc_3$ at *m/z* 1101.5 were detected in Figure 1B−D; therefore, the intensity of this signal in each spectrum was used as the guide.

MS/MS of Asn-180 Glycopeptides. To strengthen the results obtained from these exoglycosidase studies and to establish unambiguously the presence of bisecting GlcNAc on β-mannose, selected glycopeptides containing Asn-180 were subjected to low-energy MS/MS using a high-resolution hybrid quadrupole-oaTOF tandem mass spectrometer fitted with nanoelectrospray ionization. The resolution provided by this instrument enables unambiguous assignment of the charge state of each fragment ion (see inset in Figure 3), and its inherent mass accuracy ensures high confidence in sequence assignments. The fragment ion spectrum of the most abundant glycopeptide spanning Asn-180 ($Hex_4HexNAc_5Fuc_2$-$[Y_{156}-K_{184}]$; see Figure 2B) is shown in Figure 3. The spectrum is dominated by oxonium ions (B ions) at low mass, which are derived from glycosidic cleavages at the nonreducing end of the carbohydrate chain (see caption to Figure 3). Importantly, the singly charged nonreducing fragment ion at *m/z* 512.20 (for $HexFucHexNAc^+$) supports the presence of the terminal Lewis^x epitope. The absence of this signal in the MS/MS spectrum of the truncated biantennary glycopeptide comprising $Hex_3HexNAc_5Fuc$ (*m/z* 1058.3 $[M + 5H]^{5+}$) (data not shown) provides further corroboration of

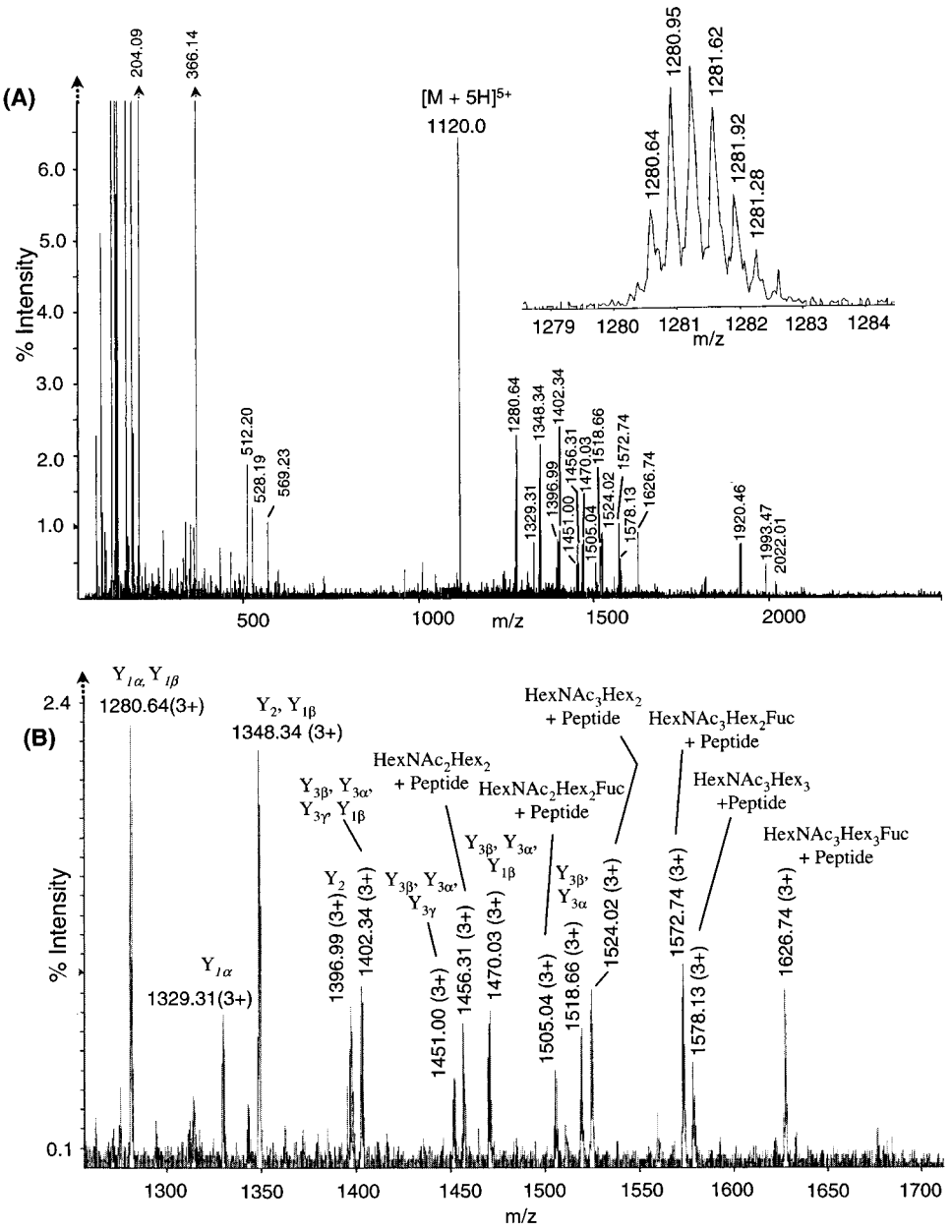

FIGURE 3: (A) CID spectrum of the glycopeptide $Hex_4HexNAc_5Fuc_2$-(Y^{156}-L^{184}) at *m/z* 1120.0 $[M + 5H]^{5+}$. The inset shows the mass resolution obtained during this experiment, which immediately enables charge state assignment. The singly charged ions at *m/z* 204.09 $(HexNAc)^+$, *m/z* 366.14 $(HexHexNAc)^+$, *m/z* 512.20 $(HexHexNAcFuc)^+$, and *m/z* 528.2 $(Hex_2HenNAc)^+$ are nonreducing terminal fragments, whereas *m/z* 569.23 $(HexHexNAc_2)^+$ is an internal ion resulting from multiple cleavages. An expanded region containing the Y ion series is shown in panel B.

this assignment. More sequence information is provided by a series of multiply charged Y ions (Figure 3B) whose formation is favored because charge is retained by the peptide attached to the reducing terminus. The collision-induced fragmentation processes observed for this glycopeptide are shown in Chart 1. The presence of the reducing terminal fragment ion $Y_{1\alpha}$ at 1329.31 $[M + 3H]^{3+}$ in all product ion spectra shows that core fucose is present on all glycopeptides analyzed. Furthermore, product ions at *m/z* 1470.03 $[M + 3H]^{3+}$ ($HexNAc_3Hex$) and *m/z* 1518.66 $[M + 3H]^{3+}$ ($HexNAc_3HexFuc$) arise from multiple Y rearrangements and establish the presence of bisecting GlcNAc on β-mannose.

Site-Specific Comparisons of the N-Linked Glycans. The glycosylation at each of the two N-linked consensus sites was directly compared via transformed spectra with intact carbohydrate mass plotted on the *x*-axis instead of glycopeptide mass. Figure 4A shows a direct comparison of the neutral components at each of the N-linked sites and reveals that the major glycoforms at Asn-180 are also present at Asn-196. However, there are many other minor neutral components at Asn-180 that are not observed on the latter site (see Figure 4A; e.g., $Hex_3HexNAc_5Fuc$ at 1666.6 Da and $Hex_5HexNAc_4Fuc_2$ at 1933.8 Da). A site-specific comparison of

Chart 1

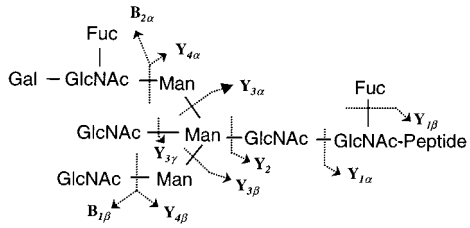

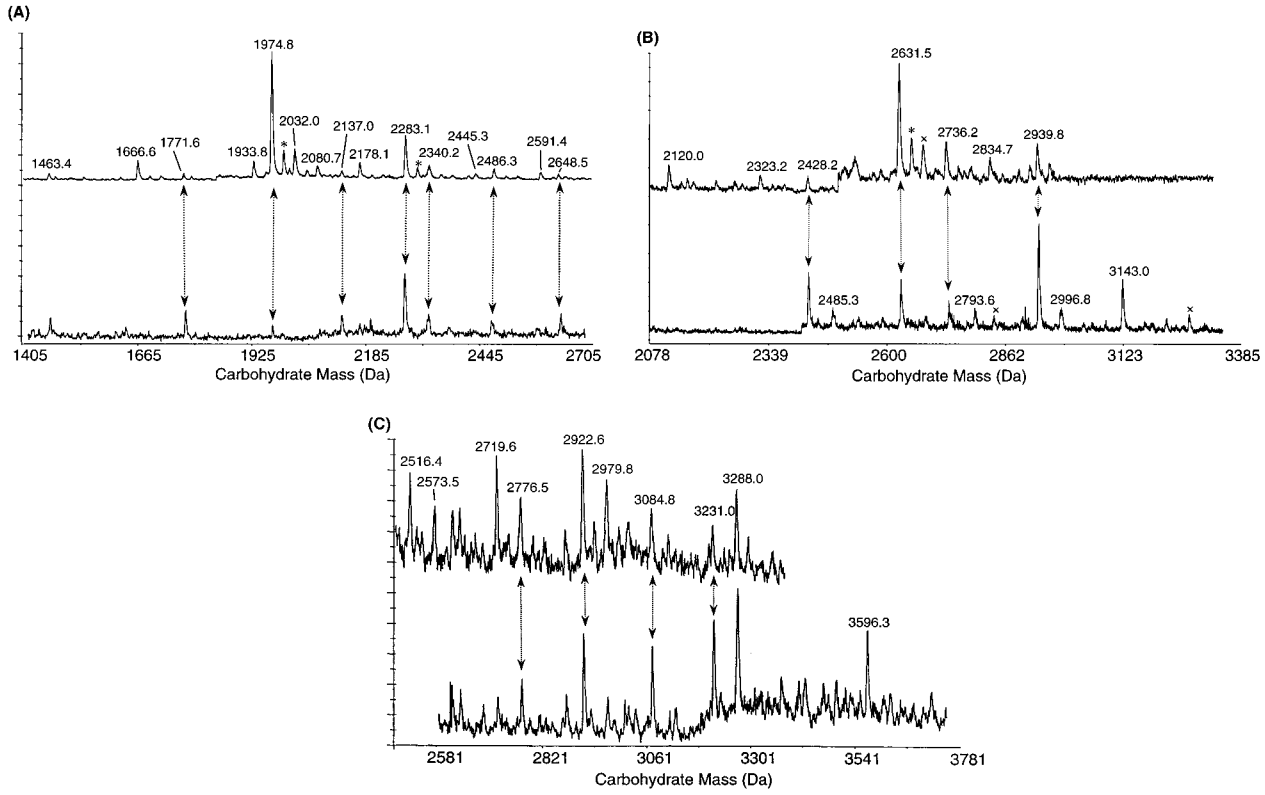

FIGURE 4: Site-specific comparisons of the (A) asialo, (B) monosialyl, and (C) disialyl oligosaccharides at Asn-180 (upper trace) and Asn-196 (lower trace). These data are presented as deconvoluted mass spectra. By plotting carbohydrate mass (daltons) instead of glycopeptide mass (daltons) along the *x*-axis, the glycans at both sites can be directly compared. Intact carbohydrate mass was calculated by subtraction of the calculated mass of the unglycosylated peptides ($Q_{185}-K_{203}$; 2137.3 Da for Asn-196 and $Y_{156}-L_{184}$; 3638.1 Da for Asn-180) from glycopeptide mass and addition of H_2O (18 Da).

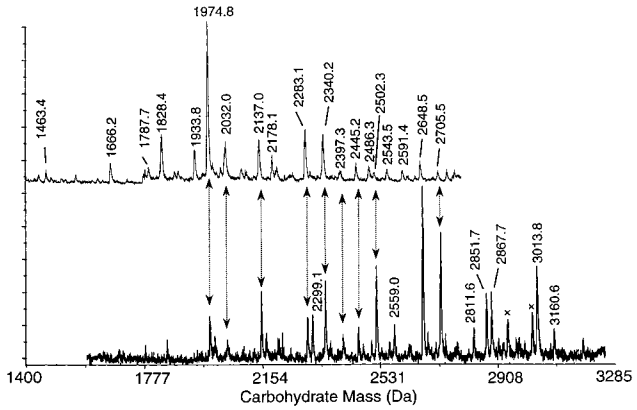

FIGURE 5: Deconvoluted mass data comparing the α-sialidase-treated oligosaccharides at Asn-180 (upper trace) and Asn-196 (lower trace) (see caption to Figure 4).

the mono- and disialylated moieties (Figure 4 panels B and C, respectively) also shows that many sialylated bi- and triantennary structures are common to both sites, although some of the larger tetraantennary structures at Asn-196 are not detected at Asn-180 (e.g., $Hex_6HexHAc_7Fuc_3NeuAc$ at 3143.0 Da and $Hex_7HexHAc_7Fuc_3NeuAc_2$ at 3596.3 Da). Asn-196 also has a significant quantity of trisialylated tri- and tetraantennary glycans that were not detected at Asn-180. A comparison of the sialidase-treated carbohydrate masses from both sites (shown in Figure 5) provides unequivocal evidence of differing N-glycan populations. It can be clearly seen that the majority of glycoforms at Asn-180 are bi- and triantennary structures falling within a mass range of approximately 1660−2340 Da. In contrast, the major glycan components at Asn-196 fall mainly within a mass range of approximately 2000 Da−3020 Da and consist of tri- and tetraantennary structures.

DISCUSSION

This work provides the first detailed site-specific structural characterization of the N-linked glycans on PrP^{Sc} by mass spectrometry. The key factor that facilitated the extensive identification of approximately 60 complex N-linked glycans was the use of a highly sensitive, three-stage mass spectrometric analysis. First, an ESI triple quadrupole mass spectrometer equipped with selected ion monitoring for carbohydrate-specific fragment ions was used to selectively detect and collect glycopeptide-containing components in a complex tryptic digest mixture (HPLC/ESI−CID-MS). Second, the isolated glycopeptide fractions were then reanalyzed by HPLC/ESI-oaTOF-MS, which permitted the detection of a myriad of glycoforms at each of the two N-linked sites. Third, more structural detail was derived for particular glycopeptide components by tandem mass spectrometry employing a ES Qq TOFMS.

The proposed structures for the N-linked complex glycans found at Asn-180 and Asn-196 from murine PrP^{Sc} are shown in Figure 6. These neutral and sialylated complex-type glycans are characterized by the presence of outer-arm α(1−3)-fucosylation (the $Lewis^x$ and sialyl-$Lewis^x$ epitopes), core α(1,6) fucose, and the presence of terminal HexNAc residues. The majority of oligosaccharides are presented with bisecting GlcNAc residues; however, additional microheterogeneity may exist arising from structural isomers that cannot be

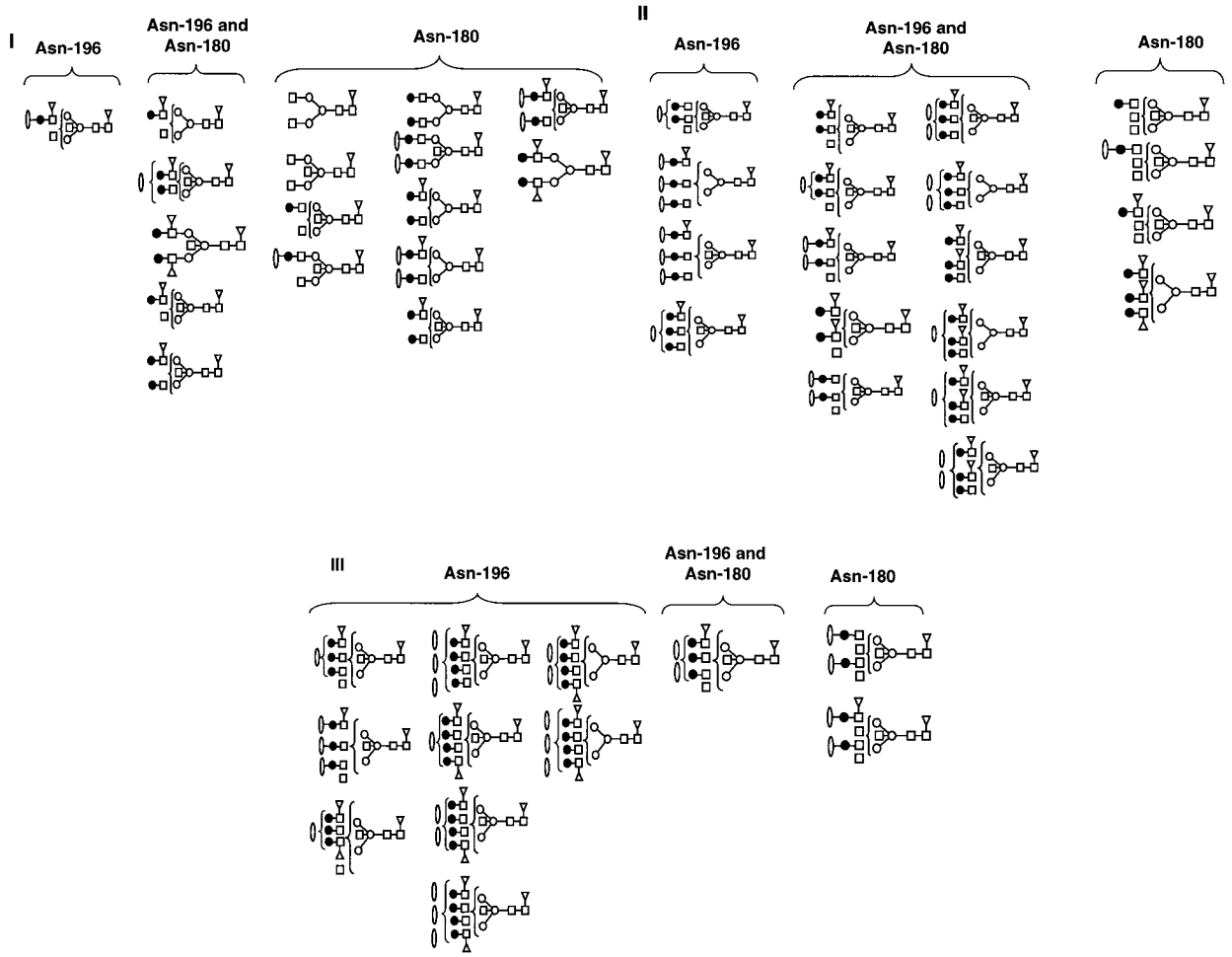

FIGURE 6: Proposed structures of the N-linked oligosaccharides at Asn-180 and Asn-196 from mouse PrP^{Sc}. Structures are grouped as (I) biantennary complex, and (II) triantennary complex, and (III) tetraantennary complex. The majority of carbohydrate structures are shown with bisecting GlcNAc and agree with the N-glycans previously characterized on hamster PrP27−30 (*3*).

characterized by MS and exoglycosidase digestions alone. For example, the oligosaccharide composition $Hex_5HexNAc_5Fuc_2$ is represented as a biantennary structure containing bisecting GlcNAc; however, a triantennary oligosaccharide with one agalactosyl antennae may also be present. Even so, the proposed N-linked glycans agree well with the information presented in previous reports on the glycosylation of hamster PrP (*3*, *4*). Furthermore, our data provide additional important structural information not revealed in earlier work. Stahl et al. (*4*) carried out a detailed mass spectrometric structural analysis of hamster PrP that facilitated the identification of the endo Lys-C glycopeptide spanning Asn-181. The structures of glycoforms observed at this hamster site and their relative abundance are directly comparable to those seen at the equivalent site on murine PrP^{Sc}. For example, the neutral biantennary structure containing one agalactosyl antenna and bisecting GlcNAc ($Hex_4HexNAc_5Fuc_2$) is by far the major glycoform on both hamster and murine PrP^{Sc}. However, the glycopeptides spanning Asn-196 were not detected and, therefore, cannot be compared with the present study. Other earlier work (*3*) on the total liberated N-glycans of hamster PrP^{Sc} established that they are composed of complex bi-, tri-, and tetraantennary structures, which all have bisecting GlcNAc, are capped with up to three sialic acid residues, and possess the $Lewis^x$ epitope, core fucosylation, and terminal and bisecting GlcNAc residues. However, the presence of the sialyl-$Lewis^x$ epitope was not unequivocally resolved and, in addition, many other glycoforms were not observed on hamster PrP, including those without bisecting GlcNAc, sialylated glycans with agalactosyl antennae, and neutral triantennary structures.

The abundance of the $Lewis^x$ and sialyl $Lewis^x$ epitopes on murine PrP^{Sc} may indicate a role for these structures in the normal function of PrP^C or the pathophysiology of PrP^{Sc}. The $Lewis^x$ trisaccharide is the major nonreducing structure at Asn-180 and significant amounts of both $Lewis^x$ and sialyl $Lewis^x$ epitopes are observed at Asn-196. The $Lewis^x$ epitope is highly regulated during development in the central nervous system. In the early chicken embryo, for example, the epitope becomes rapidly upregulated in the developing nervous system during neural induction (*17*, *18*). Furthermore, the $Lewis^x$ antigen has been suggested to serve as an intracellular recognition molecule in the developing human CNS (*16*, *17*, *19*), although no specific lectins in the CNS have been documented. In this context, PrP^c synthesis is developmentally regulated in the brain of newborn hamsters (*20*, *21*), its mRNA is widely expressed in brain and nonneural tissues during embryonic development of the mouse (*22*), and subtle deficits in nerve function are apparent in mice lacking expression of the PrP protein (*23*, *24*). The sialyl $Lewis^x$ antigen is found on the surface of leukocytes and has been identified as a ligand for the selectin family of cell adhesion molecules (*25*−*27*). However, the selectins have a relatively low affinity for the sialyl $Lewis^x$ tetrasaccharide; thus, to

attain high-affinity binding, it has been suggested that the counterreceptors might be macromolecules that present the oligosaccharides in a clustered array (*28*). Recent evidence has shown that PrP^c and PrP^{Sc} accumulate in cavolaelike membranous domains (*29*) and consequently may form clustered oligosaccharide structures within these regions on the surface neural cells. These observations raise the possibility that the Lewis^x and sialyl Lewis^x antigens on PrP may mediate interactions with target cells that express lectins recognizing these terminal sugar epitopes.

To date, much of our knowledge on the site specificity and structural elaboration for N-linked oligosaccharides has been obtained by employing glycoproteins readily isolated from serum or cell culture and recombinant glycoproteins. With few exceptions (*3*, *30*−*36*), detailed structural information of nervous tissue glycoproteins is very limited. Nevertheless, the predominant neutral structures at Asn-180 on murine PrP^{Sc} are similar to those found on the secreted neural glycoproteins such as β-trace protein and asialotransferrin (*30*, *31*). Based upon these structures, a "brain-type" signature of oligosaccharide structural features appears that is characterized by large amounts of bisecting GlcNAc, core fucosylation, outer-arm fucosylation, and agalactosyl antennae. With minor exceptions, the particular glycans attached to Asn-196 are more highly processed acidic structures and, to date, have not been observed on adult neurally derived glycoproteins. Of possible constituents of murine glycosylation, we were unable to detect any evidence for the presence of the α-galactosyl epitope that is commonly found in N-linked glycoproteins (*37*).

PrP^C is expressed primarily in neurons and, to a lesser extent, astrocytes (*38*−*40*). The nature of the N-glycans attached to PrP^{Sc} may give clues to the particular cells in which the PrP^C precursor of this PrP^{Sc} is synthesized, because the glycosyltransferases that make these complex N-glycans must also be expressed in that cell type. For example, the bisecting GlcNAc and type II lactosamine antennae of PrP may be formed by *N*-acetylglucosaminidase III (GlcNAc-TIII) (*41*) and β4-galactosyltransferase VI (β4GalT-VI) (*42*), respectively, as the mRNA of both enzymes is abundant in adult mouse brain. Of the three (α2,3)-sialyltransferases (α2,3-ST) that are known to be expressed in adult mouse brain, only one has a high specificity for oligosaccharides containing a terminal type II lactosamine chain (Galβ1−4GlcNAc) (*43*), and so this enzyme is most likely involved in the biosynthesis of the sialyl Lewis^x determinant found on PrP^{Sc}. Fucosylation of the nonreducing lactosamine moiety to form the Lewis^x epitope requires an α3-fucosyltransferase with properties similar to those reported for human and rat Fuc-TIV (*44*). However, this enzyme acts poorly on sialylated structures and therefore is unlikely to be involved in the synthesis of the sialyl-Lewis^x structure on PrP. FucT-VII is able to catalyze the synthesis of this epitope (*45*) and can generate complex selectin ligands on leukocytes (*44*), but a similar α3-fucosyltransferase capable of efficiently synthesizing the sialyl Lewis^x structure on brain glycoconjugates such as PrP remains undiscovered (*47*). Cellular variations of glycosyltransferase expression in different regions of the CNS could affect the conformation of PrP^c and account for selective targeting of PrP^{Sc}. This may also determine the rate and specific patterns of PrP^{Sc} deposition, which are characteristic of the brain pathology induced in mice infected by different strains of TSE agents (*1*, *48*). Complex glycans are present on both PrP^c and PrP^{Sc} (*49*) and ongoing studies in our laboratory will determine site-specifically whether detailed structures of glycoforms differ between strains of scrapie in murine mouse models.

ACKNOWLEDGMENT

We are indebted to Drs. Igor Chernushevich and R. Bonner of MDS Sciex, Toronto, for making their electrospray QqTOF mass spectrometer available for these studies.

REFERENCES

1. Bruce, M., Chree, A., McConnell, I., Foster, J., Pearson, G., and Fraser, H. (1994) *Philos. Trans. Roy. Soc. London, Ser. B*−*Biol. Sci. 343*, 405−411.
2. Prusiner, S. B. (1988) *Adv. Virus Res. 35*, 83−136.
3. Endo, T., Groth, D., Prusiner, S. B., and Kobata, A. (1989) *Biochemistry 28*, 8380−8388.
4. Stahl, N., Baldwin, M. A., Teplow, D. B., Hood, L., Gibson, B. W., Burlingame, A. L., and Prusiner, S. B. (1993) *Biochemistry 32*, 1991−2002.
5. Medzihradszky, K. F., Besman, M. J., and Burlingame, A. L. (1998) *Rapid Commun. Mass Spectrom. 12*, 472−478.
6. Hope, J., Multhaup, G., Reekie, L. J., Kimberlin, R. H., and Beyreuther, K. (1988) *Eur. J. Biochem. 172*, 271−277.
7. Pan, Y.-C., Wideman, J., Blacher, R., Chang, M., and Stein, S. (1984) *J. Chromatogr. 297*, 13.
8. Carr, S. A., Huddleson, M. J., and Bean, M. F. (1993) *Protein Sci. 2*, 183−196.
9. Huddleson, M. J., Bean, M. F., and Carr, S. A. (1993) *Anal. Chem. 65*, 877−884.
10. Medzihradszky, K. F., Maltby, D. A., Hall, S. C., Settineri, C. A., and Burlingame, A. L. (1994) *J. Am. Soc. Mass Spectrom. 5*, 350−358.
11. Duffin, K L, Welpy, J. K., Huang, E., and Henion, J. D. (1992) *Anal. Chem. 64*, 1440−1448.
12. Somerville, R. A., and Ritchie, L. A. (1990) *J. Gen. Virol. 71*, 833−839.
13. Burlingame, A. L., and Carr, S. A. (1996) in *Mass Spectrometry in the Biological Sciences* (Burlingame, A. L., and Carr, S. A., Eds.) pp 546−553, Humana Press, Totowa, NJ.
14. Settineri, C. A., and Burlingame, A. L. (1994) in *Techniques in Protein Chemistry V* (Crabb, J. W., Ed.) pp 97−113, Academic Press, San Diego, CA.
15. Kobata, A., and Takasaki, S. (1992) in *Cell Surface Carbohydrates and Cell Development* (Fukuda, M., Ed.) Chapter 1, CRC Press, Boca Raton, FL.
16. Hakomori, S.-I. (1992) *Histochem. J. 24*, 771−776.
17. Roberts, C., Platt, N., Streit, A. Schachner, M., and Stern, C. D. (1991) *Development 112*, 959−970.
18. Streit, A., Stern, C. D., Thery, C., Ireland, G. W., Aparicio, S., Sharpe, M. J., and Gherardi, E. (1995) *Development 121*, 823−824.
19. Eggins, I., Fenderson, B. A., Toyokuni, T., Dean, B., Stroud, M. R., and Hakamori, S. (1989) *J. Biol. Chem. 264*, 9476−9484.
20. McKinley, M. P., Hay, B., Lingappa, V. R., Lieberburg, I., and Prusiner, S. B. (1987) *Dev. Biol. 121*, 105−110.
21. Mobley, W. C., Neve, R. L., Prusiner, S. B., and McKinley, M. P. (1988) *Proc. Natl. Acad. Sci. U.S.A. 85*, 9811−9815.
22. Manson, J., West, J. D., Thomson, V., McBride, P., Kaufman, M. H., and Hope, J. (1992) *Development 115*, 117−122.
23. Whittington, M. A., Sidle, K. C. L., Gowland, I., Meads, J., Hill, A. F., Palmer, M. S., Jefferys, J. G. R., and Collinge, J. (1995) *Nat. Genet. 9*, 197−201.
24. Tobler, I., Gaus, S. E., Deboer, T., Achermann, P., Fischer, M., Rulicke, T., Moser, M., Oesch, B., McBride, P. A., and Manson, J. C. (1996) *Nature 380*, 639−642.
25. Lasky, L. A. (1995) *Annu. Rev. Biochem. 64*, 113−139.
26. Varki, A. (1994) *Proc. Natl. Acad. Sci. U.S.A. 91*, 7390−7397.

27. Rosen. S. D., and Bertozzi, C. R. (1994) *Curr. Opin. Cell Biol. 6*, 663−673.
28. Mannori, G., Crottet, P., Cecconi, O., Hanasaki, K., Aruffo, A., Nelson, R. M., Varki, A., and Becvilacqua, M. P. (1995) *Cancer Res. 55*, 4425−4431.
29. Vey, M., Pilkuhn, S., Wille, H., Nixon, R., DeArmond, S. J., Smart, E. J., Anderson, R. G. W., Taraboulos, A., and Prusiner, S. B. (1996) *Proc. Natl. Acad. Sci. U.S.A. 93*, 14945−14949.
30. Hoffman, A., Nimtz, M., Wurster, U., and Conradt, H. S. (1994) *J. Neurochem. 63*, 2185−2196.
31. Hoffman, A., Nimtz, M., Getzlaff, R., and Conradt, H. S. (1995) *FEBS Lett. 359*, 164−168.
32. Taniguchi, T., Adler, A. J., Mizuochi, T., Kochiba, N., and Kobata, A. (1986) *J. Biol. Chem. 261*, 1730−1736.
33. Voshel, H., van Zuylen, W. E. M., Orberger, G., Vliegenthart, J. F. G., and Schachner, M. (1996) *J. Biol. Chem. 271*, 22957−22960.
34. Chen, Y.-J., Wing, D. R., Guile, G. R., Dwek, R. A., Harvey, D. J., and Zamze, S. (1998) *Eur. J. Biochem. 251*, 691−703.
35. Parekh, R. B., Tse, A. G. D., Dwek, R. A., Williams, A. H., and Rademacher, T. W. (1987) *EMBO J. 6*, 1233−1244.
36. Kudo, M., Kitajima, K., Inoue, S., Shiokawa, K., Morris, H. R., Dell, A., and Inoue, Y. (1996) *J. Biol. Chem. 51*, 32667−32677.
37. Galili, U., Clark, M. R., Shohet, S. B., Buehler, J., and Macher, B. A. (1987) *Proc. Natl. Acad. Sci. U.S.A. 84*, 1369−1373.
38. Kretzschmar, H. A., Prusiner, S. B., Stowring, L. E., and DeArmond, S. J. (1986) *Am. J. Pathol. 122*, 1−5.
39. Manson, J., McBride, P., and Hope, J. (1992) *Neurodegeneration 1*, 45−52.
40. Moser, M., Colello, R. J., Pott, U., and Oesch, B. (1995) *Neuron 14*, 509−517.
41. Bhaumik, M., Seldin, M. F., and Stanley, P. (1995) *Gene 164*, 295−300.
42. Lo, N.-W, Sahper, J. H., Pevsner, J., and Shaper, N. L. (1998) *Glycobiology 8*, 517−526.
43. Tsuji, S. (1996) *J. Biochem. (Tokyo) 120*, 1−13.
44. Wiederschain, G., Koul, O., Bovin, N., Nifantev, N., and McCluer, R. (1996) *Glycobiology 6*, 761.
45. Wagers, A. J., Lowe, J. B., and Kansas, G. S. (1996) *Blood 88*, 2125−2132.
46. Britten, C. J., van den Eijnden, D. H., McDowel, W., Kelly, V. A., Witham, S. J., Smith, P. L., Gersten, K. M., Petryniak, B., Kelly, R. J., Rogers, C., Natsuka, Y., Alford, J. A., III, Scheidegger, P. E., Natsuka, S., and Lowe, J. B. (1996) *J. Biol. Chem. 271*, 8250−8259.
47. Smith, P. L., Gersten, K. M., Petryniak, B., Kelly, R. J., Rogers, C., Natsuka, Y., Alfor, J. A., III, Scheidegger, P., Natsuka, S., and Lowe, J. B. (1996) *J. Biol. Chem. 271*, 8250−8259.
48. DeArmond, S. J., Sanchez, H., Yehiely, F., Qui, Y., Ninchak-Casey, A., Daggett, V., Camerino, A. P., Cayetano, J., Rogers, M., Groth, D., Torchia, M., Tremblay, P., Scott, M. R., Cohen, F. E., and Prusiner, S. B. (1997) *Neuron 19*, 1337−1348.
49. Haraguchi, T., Fisher S. J., Olofsson, S., Endo, T., Groth, D., Tarentino, A., Borchelt, D., Teplow, D., Hood, L., Burlingame, A. L., Lycke, E., Kobata, A., and Prusiner, S. B. (1989) *Arch. Biochem. Biophys. 274*, 1−13.

BI982330Q